



Efficient nondoped blue organic light-emitting diodes based on phenanthroimidazole-substituted anthracene derivatives

Shaoqing Zhuang^{a,c}, Ronggang Shangguan^a, Jiangjiang Jin^a, Guoli Tu^a, Lei Wang^{a,*}, Jiangshan Chen^{b,*}, Dongge Ma^b, Xunjin Zhu^{c,*}

^a Wuhan National Laboratory for Optoelectronics, Huazhong University of Science and Technology, Wuhan 430074, People's Republic of China

^b State Key Laboratory of Polymer Physics and Chemistry, Changchun Institute of Applied Chemistry, Chinese Academy of Sciences, Changchun 130022, People's Republic of China

^c Centre for Advanced Luminescence Materials, Department of Chemistry, Hong Kong Baptist University, Waterloo Road, Hong Kong, People's Republic of China

ARTICLE INFO

Article history:

Received 31 May 2012

Received in revised form 12 July 2012

Accepted 20 August 2012

Available online 6 September 2012

Keywords:

Blue material

Anthracene

Phenanthroimidazole

Organic light-emitting devices

ABSTRACT

A series of new blue materials based on highly fluorescent di(aryl)anthracene and electron-transporting phenanthroimidazole functional cores: 2-(4-(anthracen-9-yl)phenyl)-1-phenyl-1H-phenanthro[9,10-d]imidazole (**ACPI**), 2-(4-(10-(naphthalen-1-yl)anthracen-9-yl)phenyl)-1-phenyl-1H-phenanthro[9,10-d]imidazole (**1-NaCPI**), 2-(4-(10-(naphthalen-2-yl)anthracen-9-yl)phenyl)-1-phenyl-1H-phenanthro[9,10-d]imidazole (**2-NaCPI**) were designed and synthesized. These materials exhibit good film-forming and thermal properties as well as strong blue emission in the solid state. To explore the electroluminescence properties of these materials, three layer, two layer and single layer organic light-emitting devices were fabricated. With respect to the three layer device **4** using **ACPI** as the emitting layer, its maximum current efficiency reaches 4.36 cd A^{-1} with Commission Internationale de l'Eclairage (CIE) coordinates of (0.156, 0.155). In the single layer device **10** based on **ACPI**, maximum current efficiency reaches 1.59 cd A^{-1} with Commission Internationale de l'Eclairage (CIE) coordinates of (0.169, 0.177). Interestingly, both device **4** and **10** has low turn on voltage and negligible efficiency roll off at high current densities.

© 2012 Elsevier B.V. All rights reserved.

1. Introduction

Since the pioneering work by Tang and Van Slyke [1], significant progresses in materials and device engineering have led to the potential application of full-color OLEDs and solid-state lighting [2]. For full-color displays, it is essential to have the three primary colors, red, green and blue. Red and green phosphorescent electroluminescent devices with high efficiencies, long lifetimes, and proper CIE coordinates have been well developed. However, blue phosphorescent devices are still the bottleneck for the high CIE coordinates (y -coordinate value >0.30) and short device lifetime [3]. Therefore, to achieve marketable OLEDs,

the hunt for blue fluorescent materials and devices are still a subject of current interest [4].

Based on anthracene, a well-known building block and starting material in OLEDs, new diverse of blue material and corresponding devices have been reported previously [5]. For example, Park group [6] have synthesized carbazole-based anthracene derivatives 3,6-di(anthracen-9-yl)-9-phenyl-9H-carbazole (P-DAC) and attained device efficiency of 3.14 cd A^{-1} , color coordinates (0.16, 0.14), and threshold voltage 3.8 V. Li's team [7] have shown fluorene based naphthylanthracene derivatives with a maximum luminance efficiency of 4.04 cd A^{-1} , CIE coordinates of (0.15, 0.13) and a turn on voltage of 4.1 V. Recently, phenanthroimidazole derivatives have attracted great attention as electroluminescent materials because of their high thermal stability and efficient electron transporting ability. Huang's group [8] reported bis(phenanthroimidazolyl)biphenyl

* Corresponding authors. Tel./fax: +86 27 87793032 (L. Wang).

E-mail addresses: wanglei@mail.hust.edu.cn (L. Wang), jschen@ciac.jl.cn (J. Chen), xjzhu@hkbu.edu.cn (X. Zhu).

derivatives as excellent non-doped blue emitting materials with optimized device efficiency of 7.3 lm W^{-1} , CIE coordinates of (0.15, 0.14). By using phenanthroimidazole as a building block for luminescent materials, Ma's group [9] also reported pure blue devices with luminance efficiency of 6.87 cd A^{-1} , CIE coordinates of (0.15, 0.21) and a turn on voltage of 2.8 V. Although these relatively successful blue materials were reported, many of them, the efficiency roll off at high current densities, so it is still a great need to design and synthesize stable blue materials which exhibit little efficiency roll off at high current densities [4a,5a,5b,5e,8]. One of the basic designs for blue materials is to increase their electron affinities to realize balanced charge injection and transport [8,9]. It should be noted that, in spite of increasing electron transporting properties, the incorporation of electron-withdrawing moiety in those saturated blue-emitted materials always results in lower HOMO levels, which mismatch with side layer and generate larger hole-injection barriers at the hole-transporter/emitter junctions. Hence, in designing pure blue light emitting materials for OLEDs, a compromise is needed between electron transporting ability and adjusting the HOMO/LUMO levels.

In previous work [10,11], we have introduced electron-rich benzothiophene or fluorene moieties into anthracene, to adjust the emitter's HOMO/LUMO level and carrier transporting ability. Here, we designed and synthesized three asymmetric phenanthroimidazole-substituted anthracene derivatives. The introduction of phenanthroimidazole moieties effectively increases the electron injection and transport ability and finely adjusts the ionization potentials (Ip) of the compounds, and further reduces the hole injection barrier at the interface of the hole-transporting layer (HTL) and the emissive layer and balanced recombination [12]. As expected, these materials show perfect thermal stability and excellent EL performance with low onset voltages, which indicate that these new materials are a promising class of blue emitters for practical applications in panel display.

2. Experimental section

2.1. Materials and methods

All reagents and solvents were used as purchased from Aldrich and were used without further purification. $^1\text{H-NMR}$ spectra were recorded using a Bruker-AF301 at 400 MHz. Mass spectra were carried out on an Agilent (1100 LC/MSD Trap) using APCI ionization. Elemental analyses of carbon, hydrogen, and nitrogen were performed on an Elementar (Vario Micro cube) analyzer. Fluorescence spectra were obtained on Edinburgh instruments (FLSP920 spectrometers) and UV-Vis spectra were measured using a Shimadzu UV-VIS-NIR Spectrophotometer (UV-3600). The differential scanning calorimetry (DSC) analysis was performed under a nitrogen atmosphere at a heating rate of $10 \text{ }^\circ\text{C}/\text{min}$ using a PE Instruments DSC 2920. Thermogravimetric analysis (TGA) was undertaken using a PerkinElmer Instruments (Pyris1 TGA) under nitrogen atmosphere at a heating rate of $10 \text{ }^\circ\text{C}/\text{min}$. AFM was measured using Veeco

(DIMENSION 3100). To measure the PL quantum yields (Φ_f), degassed solutions of the compounds in CH_2Cl_2 were prepared. The concentration was adjusted so that the absorbance of the solution would be between 0.05 and 0.1. The excitation was performed at 330 nm and 9,10-diphenylanthracene (DPA) in cyclohexane ($\Phi = 0.9$ in cyclohexane) was used as a standard [13]. Cyclic voltammetry measurements were carried out in a conventional three electrode cell using a Pt button working electrode of 2 mm in diameter, a platinum wire counter electrode, and a Ag/AgNO_3 (0.1 M) reference electrode on a computer-controlled EG&G Potentiostat/Galvanostat model 283 at room temperature. Oxidations CV of all compounds were performed in dichloromethane containing 0.1 M tetrabutylammoniumhexafluorophosphate (Bu_4NPF_6) as the supporting electrolyte. The onset potential was determined from the intersection of two tangents drawn at the rising and background current of the cyclic voltammogram and calibrated to the ferrocene/ferrocenium (Fc/Fc^+) redox couple. DFT calculations have been performed to characterize the 3D geometries and the frontier molecular orbital energy levels of ACPI, 1-NaCPI and 2-NaCPI at the B3LYP/6-31G* level by using the ADF2009.01 program.

2.2. Preparation of compounds

2.2.1. Synthesis of compound 1

A 250 ml round-bottomed flask was charged with 9,10-phenanthrenequinone (2.08 g, 10 mmol), aniline (0.93 g, 10 mmol), 4-bromobenzaldehyde (1.85 g, 10 mmol) and ammonium acetate (9.24 g, 120 mmol) under nitrogen atmosphere. Subsequently, 120 mL acetic acid was added to the solution and the reaction mixture was stirred under reflux for 36 h under an argon atmosphere. After cooled to room temperature, the mixture was poured into water. The separated solid was filtered off, washed with methanol and dried to give a white solid without further purification. Yield 3.68 g (82%). $^1\text{H-NMR}$: (DMSO- d_6 , 400 MHz): δ (ppm) 8.94 – 8.91 (d, $J = 8.4 \text{ Hz}$, 1H), 8.89 – 8.86 (d, $J = 8.4 \text{ Hz}$, 1H), 8.71 – 8.68 (dd, $J = 1.2, 8.0 \text{ Hz}$, 1H), 7.80 – 7.67 (m, 7H), 7.58 – 7.54 (m, 3H), 7.51 – 7.49 (dd, $J = 2.0, 6.8 \text{ Hz}$, 2H), 7.51 – 7.49 (t, $J = 7.2 \text{ Hz}$, 1H), 7.09 – 7.07 (d, $J = 8.0 \text{ Hz}$, 1H). MS (APCI) (m/z): $[\text{M}+\text{H}^+]$ calcd for $\text{C}_{27}\text{H}_{18}\text{-BrN}_2$, 450.3; found, 450.4.

2.2.2. Synthesis of compound ACPI

A 100 ml two-neck round-bottomed flask was added compound 1 (0.90 g, 2 mmol), anthracen-9-ylboronic acid (0.49 g, 2.2 mmol), toluene (30 ml), ethanol (15 ml), 2 M K_2CO_3 (30 ml, 60 mmol) aqueous solution and tetrakis-(triphenylphosphine) palladium (0) (0.12 g, 0.1 mmol) in turn, then the reaction mixture was refluxed under nitrogen for 24 h in the absence of light. After the reaction was completed, cooled to room temperature. The solution was extracted with dichloromethane, dried by MgSO_4 . The organic layer was concentrated under a reduced pressure and purified by column chromatography and dried under vacuum to yield a white solid. Yield: 90%. $^1\text{H-NMR}$: (DMSO- d_6 , 400 MHz): δ (ppm) 8.95 – 8.93 (d, $J = 8.0 \text{ Hz}$, 1H), 8.90 – 8.88 (d, $J = 8.0 \text{ Hz}$, 1H), 8.79 – 8.76 (d, $J = 8.0 \text{ Hz}$, 1H), 8.66 (s, 1H), 8.15 – 8.12 (d, $J = 8.0 \text{ Hz}$,

2H), 7.84–7.77 (m, 5H), 7.76–7.68 (m, 4H), 7.59–7.46 (m, 5H), 7.44–7.33 (m, 5H), 7.15–7.13 (d, $J=8.0$ Hz, 1H). MS (APCI) (m/z): $[M+H^+]$ calcd for $C_{41}H_{27}N_2$, 547.7; found, 547.2. ^{13}C NMR (100 MHz, DMSO- d_6) δ (ppm) 150.68, 139.14, 138.75, 137.10, 135.92, 131.31, 131.25, 130.90, 130.81, 130.14, 129.79, 129.69, 129.60, 129.65, 128.94, 128.40, 128.23, 128.00, 127.25, 127.14, 126.46, 126.27, 126.23, 125.80, 125.75, 125.00, 124.17, 123.00, 122.53, 120.72. Anal. Calcd for $C_{41}H_{26}N_2$: C, 90.08; H, 4.79; N, 5.12. Found: C, 89.90; H, 4.89; N, 5.21.

2.2.3. Synthesis of compound 1-NaCPI

The compound was synthesized using a similar procedure as for compound ACPI, yield: 85%. 1H -NMR: (DMSO- d_6 , 400 MHz): δ (ppm) 8.99–8.97 (d, $J=8.0$ Hz, 1H), 8.94–8.92 (d, $J=8.0$ Hz, 1H), 8.79–8.77 (d, $J=8.0$ Hz, 1H), 8.21–8.19 (d, $J=8.0$ Hz, 1H), 8.15–8.13 (d, $J=8.0$ Hz, 1H), 7.96–7.71 (m, 10H), 7.62–7.51 (m, 7H), 7.46–7.28 (m, 8H), 7.17–7.15 (d, $J=8.0$ Hz, 1H), 6.94–6.92 (d, $J=8.0$ Hz, 1H). MS (APCI) (m/z): $[M+H^+]$ calcd for $C_{41}H_{27}N_2$, 547.7; found, 547.2. ^{13}C NMR (100 MHz, CDCl $_3$) δ (ppm) 136.68, 136.59, 135.31, 133.71, 133.58, 131.45, 131.40, 130.61, 130.29, 130.03, 129.76, 129.45, 129.25, 129.19, 128.40, 128.25, 128.16, 127.41, 127.11, 126.85, 126.61, 126.38, 126.29, 126.02, 125.77, 125.59, 125.22, 125.04, 124.20, 123.17, 123.06, 122.93, 120.96. Anal. Calcd for $C_{51}H_{32}N_2$: C, 91.04; H, 4.79; N, 4.16. Found: C, 90.61; H, 4.87; N, 4.33.

2.2.4. Synthesis of compound 2-NaCPI

The compound was synthesized using a similar procedure as for compound ACPI. Yield: 90%. 1H -NMR: (DMSO- d_6 , 400 MHz): δ (ppm) 8.97–8.95 (d, $J=8.0$ Hz, 1H), 8.92–8.90 (d, $J=8.0$ Hz, 1H), 8.80–8.77 (d, $J=8.0$ Hz, 1H), 8.20–8.17 (d, $J=8.0$ Hz, 1), 8.13–8.10 (d, $J=8.0$ Hz, 1H), 8.04–8.01 (d, $J=10.0$ Hz, 2H), 7.90–7.70 (m, 9H), 7.67–7.54 (m, 8H), 7.79–7.35 (m, 7H), 7.17–7.14 (d, $J=8.0$ Hz, 1H). MS (APCI) (m/z): $[M+H^+]$ calcd for $C_{51}H_{33}N_2$, 673.8; found, 673.5. ^{13}C NMR (100 MHz, DMSO- d_6) δ (ppm) 150.70, 139.38, 138.78, 137.18, 137.11, 136.35, 136.08, 133.50, 132.86, 131.37, 130.95, 130.88, 130.28, 130.25, 129.84, 129.74, 129.67, 129.55, 129.07, 128.60, 128.46, 128.29, 128.24, 128.03, 127.25, 127.18, 127.12, 127.04, 126.67, 126.31, 126.20, 126.14, 125.78, 125.04, 124.21, 123.02, 122.52, 120.73. Anal. Calcd for $C_{51}H_{32}N_2$: C, 91.04; H, 4.79; N, 4.16. Found: C, 90.61; H, 4.87; N, 4.33.

2.3. Device fabrication and measurement

The EL devices were fabricated by vacuum deposition of the materials at a base pressure of 5×10^{-6} Torr onto glass precoated with a layer of indium tin oxide (ITO) with a sheet resistance of 25 Ω /square. Before deposition of an organic layer, the clear ITO substrates were treated with oxygen plasma for 5 min. The deposition rate of organic compounds was 0.9–1.1 $\text{\AA} \text{ s}^{-1}$. Finally, a cathode composed of cesium pivalate (2 nm) and aluminum (100 nm) was sequentially deposited onto the substrate in the vacuum of 10^{-5} Torr. The L – V – J of the devices was measured with a Keithley 2400 Source meter and PR655. All measurements were carried out at room temperature under ambi-

ent conditions. By the way, in counting the layers of the device, we only consider the hole transport layer, emissive layer and electron transport layer.

3. Results and discussion

3.1. Synthesis

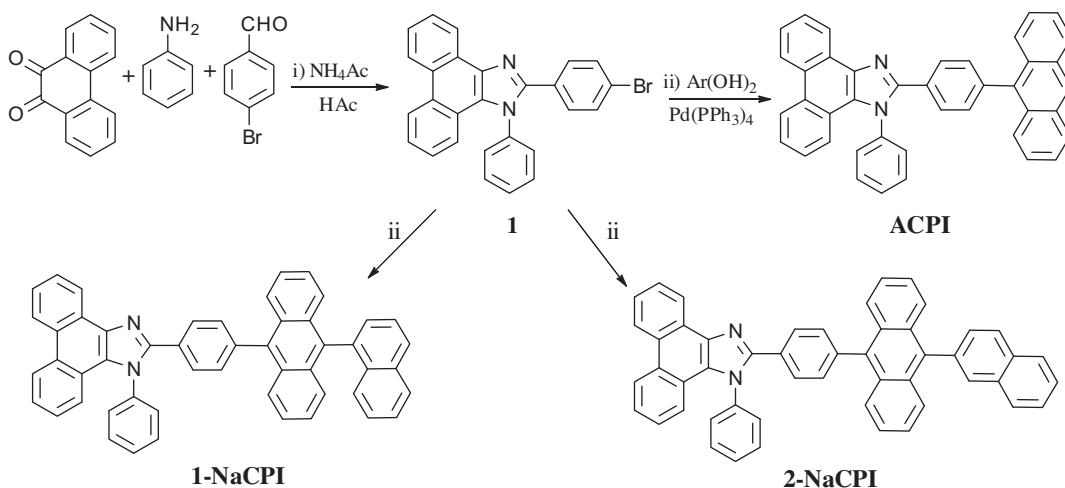
The structures and synthetic routes of the three well-defined compounds are shown in Scheme 1. Anthracene-9-ylboronic acid, 9-(1-naphthyl)anthracene-10-boronic acid, and 9-(2-naphthyl)anthracene-10-boronic acid were synthesized according to the literature [14]. The intermediate 2-(4-bromophenyl)-1-phenyl-1H-phenanthro[9,10-d]-imidazole was synthesized in high yield [12]. The title products were prepared through the palladium-catalyzed Suzuki coupling reaction of the intermediate and the corresponding aryl boronic acid, then purified by column chromatography on silica gel using petroleum ether-dichloromethane as the eluent. Repeated temperature-gradient vacuum sublimation are required for further purification of these materials used in OLEDs. All the new compounds were fully characterized by 1H and ^{13}C NMR, mass spectrometry, and elemental analysis.

3.2. Thermal properties

The thermal properties of the three compounds were investigated by thermal gravimetric analysis (TGA) and differential scanning calorimetry (DSC) under a nitrogen atmosphere, and the related data are listed in Table 1. Compounds ACPI, 1-NaCPI and 2-NaCPI exhibit good thermal stability with decomposition temperatures (T_d , 5% weight loss) at 410, 441 and 473 $^\circ\text{C}$, respectively. As shown in Fig. 1, no obvious glass transition temperatures (T_g) are observed for the three molecules, while endothermic melting transition temperatures (T_m) appear obviously at 290, 345 and 354 $^\circ\text{C}$ for ACPI, 1-NaCPI and 2-NaCPI, respectively. Such high T_m and T_d values indicate that these compounds are stable and has the potential to be fabricated into devices by vacuum thermal evaporation technology, which is highly desirable for high performance OLED applications.

3.3. Morphology properties

Since efficient film-forming properties of light emitting materials are crucial for the performance of the devices, the surface morphologies of vacuum-deposited thin films of the three new compounds, ACPI, 1-NaCPI and 2-NaCPI, were studied by atomic force microscopy (AFM). For a direct comparison, we prepared both unannealed films and thermally annealed samples films at 120 $^\circ\text{C}$ for 2 h under an N_2 atmosphere. As shown in Fig. 2, the unannealed film samples exhibit a root-mean-square (RMS) roughness of 0.361, 0.384 and 0.280 nm for ACPI, 1-NaCPI and 2-NaCPI, respectively. The annealed film exhibits a fairly smooth surface morphology with a root-mean-square (RMS) roughness of 0.283, 0.321 and 0.274 nm for ACPI, 1-NaCPI and 2-NaCPI, respectively. The small RMS difference



Scheme 1. Synthetic route of **ACPI**, **1-NaCPI** and **2-NaCPI**. Reagents and conditions: (i) NH_4Ac , HAc , reflux; (ii) toluene, K_2CO_3 , ethanol, aryl boric acid, $\text{Pd}(\text{PPh}_3)_4$, reflux.

Table 1

The optical, photophysical and thermal properties of **ACPI**, **1-NaCPI**, and **2-NaCPI**.

Compound	HOMO/LUMO (eV) ^a	HOMO/LUMO (eV) ^b	Φ_F	E_g (eV)	E_{ox} (V)	PL (nm)		Abs (nm)	$T_g/T_m/T_d$ (°C)
						Solution	Film		
ACPI	−5.62/−2.54	−5.30/−2.29	0.87	3.08	0.82	427	456	349, 367, 387	ND/290/410
1-NaCPI	−5.58/−2.56	−5.25/−2.35	0.71	3.02	0.78	431	455	358, 376, 396	ND/345/441
2-NaCPI	−5.55/−2.55	−5.24/−2.29	0.64	3.00	0.75	437	457	359, 376, 396	ND/354/473

^a Determined from the onset of oxidation potentials and the $E_g = \text{HOMO} - \text{LUMO}$.

^b Values from DFT calculation.

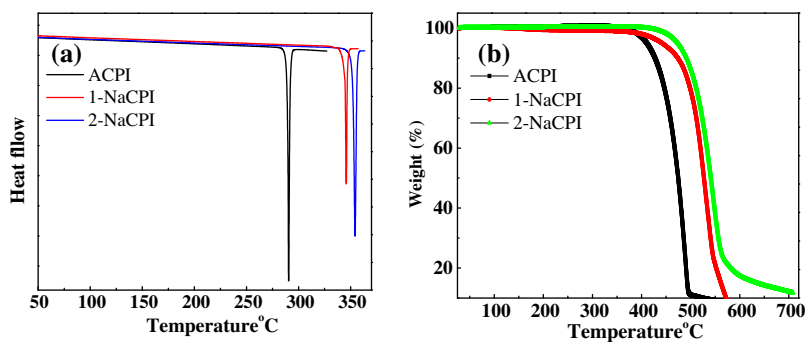


Fig. 1. (a) DSC curves of **ACPI**, **1-NaCPI** and **2-NaCPI**; (b) TGA curves of **ACPI**, **1-NaCPI** and **2-NaCPI**.

between unannealed and annealed film samples suggests their excellent thermal and amorphous stability, which indicates that attaching phenanthroimidazole moiety to anthracene's 9-position may influence the arrangement of the molecules in the thin films and makes them desirable for good performance OLEDs.

3.4. Theoretical calculations

The three-dimensional geometries and the frontier molecular orbital energy levels of these compounds were calculated using density functional theory. The resulted

HOMO and LUMO levels are depicted in Table 1. As shown in Fig. 3, the spatial distributions of electron densities of HOMO and LUMO for all the three compounds are mostly localized on the anthracene units, it implies that the absorption and emission process may mainly be attributed to the $\pi - \pi^*$ transition centered at the anthracene moiety. The HOMO level of ACPI, 1-NaCPI and 2-NaCPI locate at −5.30, −5.25 and −5.24 eV, respectively. The HOMO levels for ACPI, 1-NaCPI and 2-NaCPI increase about 0.04–0.05 eV for the elongation of conjugation when introducing naphthyl group on the 9-position of anthracene of ACPI. In addition, the calculated geometries of ACPI, 1-NaCPI and 2-

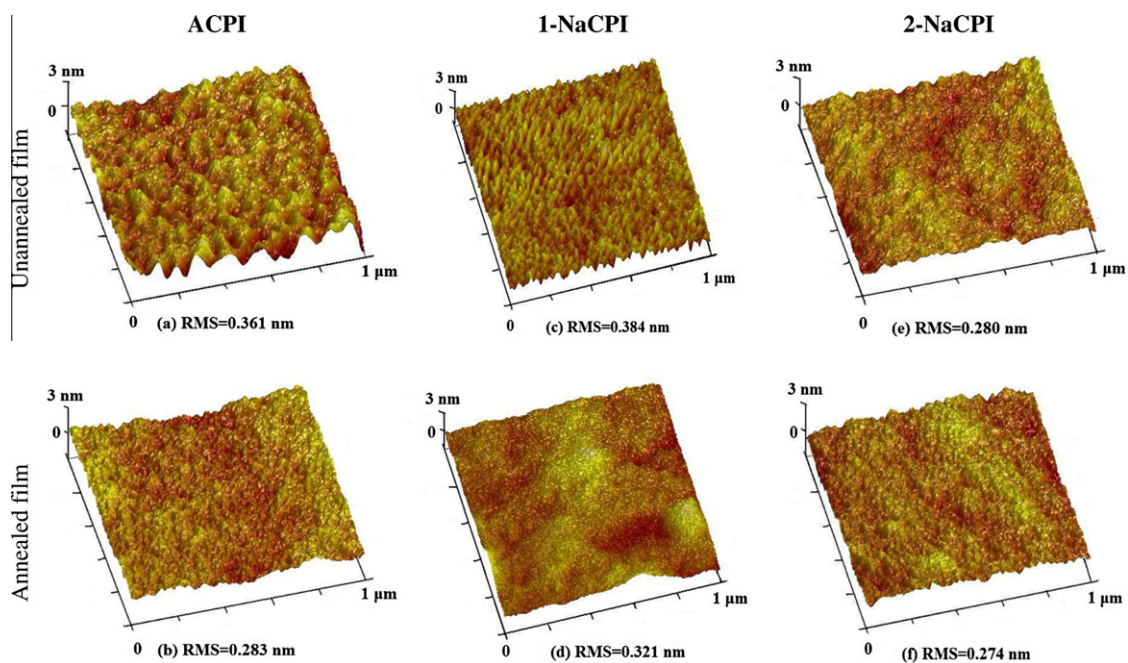


Fig. 2. AFM topographic images of the three compounds in unannealed and annealed films.

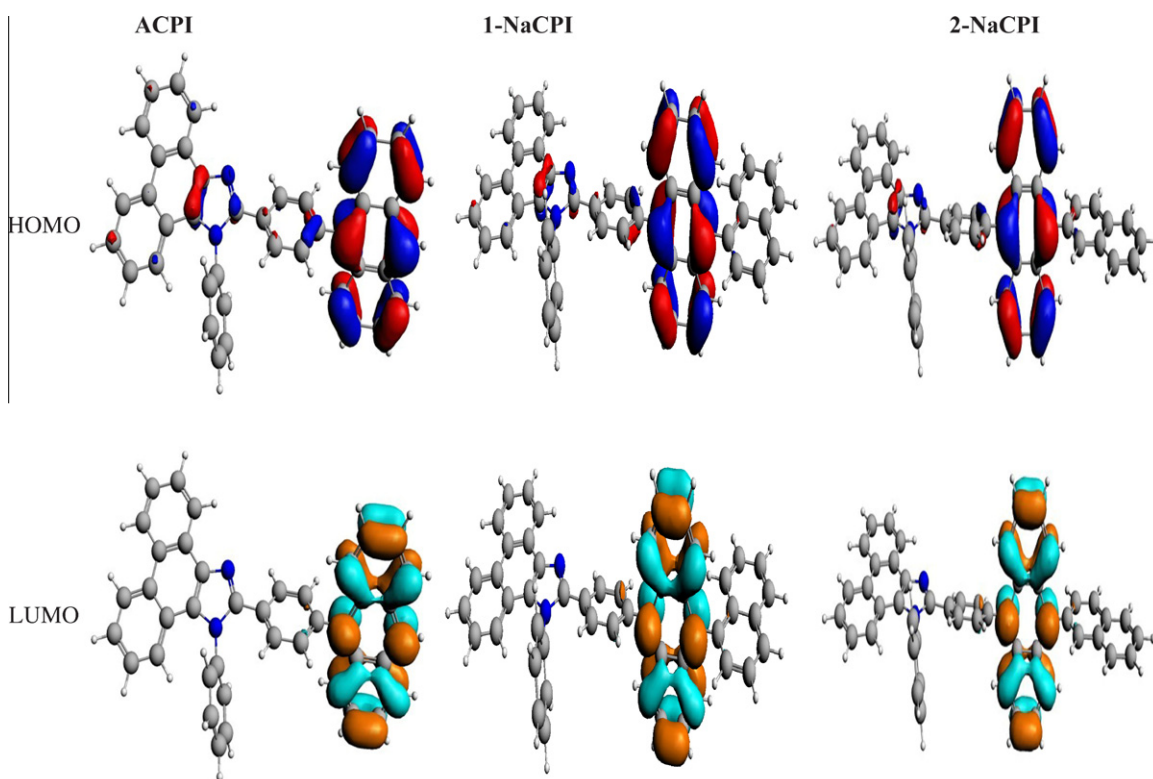


Fig. 3. Three-dimensional structures and calculated HOMO and LUMO density maps of ACPI, 1-NaCPI and 2-NaCPI.

NaCPI indicate the non-planarity of their molecular structures. These geometrical characteristics can effectively prevent intermolecular interactions between π -systems and, thus, suppress molecular recrystallization.

3.5. Photophysical properties

Fig. 4(a) shows the UV–Vis spectra of compounds ACPI, 1-NaCPI and 2-NaCPI at room temperature in a CH_2Cl_2

solution. And Fig. 4(b) shows the fluorescence spectra of compounds ACPI, 1-NaCPI and 2-NaCPI at room temperature in both CH_2Cl_2 solution and solid state. The related photophysical properties are summarized in Table 1. All of these compounds have similarly structured absorption spectra in the range of 380–425 nm in solution, which are assigned to the π - π^* transition of the characteristic vibrational structures of the isolated anthracene groups. The 10 nm blue shift of ACPI compared to 1-NaCPI and 2-NaCPI can be attributed to its short conjugation. And upon excitation at 330 nm, the maximum emission wavelengths of ACPI, 1-NaCPI and 2-NaCPI in CH_2Cl_2 solution were observed at 427, 431 and 437 nm, respectively. Compared with ACPI, 1-NaCPI and 2-NaCPI show bathochromic shifts of 4 and 10 nm respectively, due to the lengthened conjugation by the naphthalene group. On the other side, the greater steric hindrance of 1-naphthyl than 2-naphthyl leads to an increasing non-planarity property of naphthalene ring to anthracene group, which also annotate that 2-NaCPI shows larger bathochromic shift than 1-NaCPI [14]. The maximum emission peaks of ACPI, 1-NaCPI and 2-NaCPI in thin films are red-shifted by 29, 24 and 20 nm respectively, compared to the corresponding ones in CH_2Cl_2 solution. These features are reasonable for organic and polymer materials due to intermolecular interactions or exciton hopping in the solid state [15]. Moreover, a gradual decreasing red-shift effects was observed with an increasing elongation of conjugation, ACPI (29 nm) > 1-NaCPI (24 nm) > 2-NaCPI (20 nm). The quantitative enhancement of emission was evaluated by the PL quantum yields (Φ_F), using 9,10-diphenylanthracene as a standard. In toluene, blue emitters ACPI, 1-NaCPI and 2-NaCPI exhibit quantum yields of 0.87, 0.71 and 0.62, respectively. Therefore, these compounds are excellent candidates for using as efficient emitting materials in OLEDs.

3.6. Electrochemical properties

In addition to the photophysical properties, the electrochemical properties are also very important in evaluating a material's usefulness for optoelectronic applications. The electrochemical behaviors of the compounds ACPI, 1-NaCPI and 2-NaCPI were examined by cyclic voltammetry using a standard three-electrode electrochemical cell in an electrolyte solution of 0.1 M tetrabutylammoniumhexafluoro-

phosphate (Bu4NPF6) dissolved in dichloromethane (Fig. 5). The onset oxidation peaks (E_{ox}) for the three compounds are 0.82, 0.78, and 0.75 eV versus the ferrocenium/ferrocene redox couple, respectively. Thus, the HOMO levels were determined to be -5.62 , -5.58 and -5.55 eV respectively (Table 1) by the method $-(E_{ox} + 4.80)$ eV reported by Chen [16]. The HOMO levels for both 1-NaCPI and 2-NaCPI with a peripheral naphthalene group are lower than that of ACPI. It could be rationalized that the electron-donating substituent might reduce the oxidation potentials of the molecule and increase the HOMO energy level. This trend is in good agreement with the calculated values. The lower energy barrier between emitting layer of 1-NaCPI or 2-NaCPI and the hole transporting layer will facilitate hole injection into the emission layer.

3.7. Electroluminescence

To explore the electron injection and transport ability of ACPI, 1-NaCPI and 2-NaCPI, an electron-only devices with configuration: Al (100 nm)/TPBI(40 nm)/ACPI, 1-NaCPI or 2-NaCPI or m-ADN (40 nm)/LiF (1 nm)/Al (100 nm) were fabricated, respectively. For the electron-only devices, the TPBI layer, which has a low-lying HOMO level of -6.2 eV, was used to prevent hole-injection from the Al anode (-4.3 eV) to the organic layers. Here, a typical anthracene derivative 2-methyl-9,10-di(naphthalen-2-yl)anthracene (m-ADN) was used as a stand. All of the three new compounds exhibit higher current density than m-ADN at the same voltage (see Supplementary Data Fig. S1), which means the introduction of phenanthroimidazole group to anthracene increases the electron injection and transport ability of anthracene.

To evaluate the EL performances of ACPI, 1-NaCPI and 2-NaCPI as blue emitters, three type (three layer: anode/HTL/emitter/ETL/cathode, two layer: anode/HTL/emitter/cathode, Single layer: anode/emitter/cathode), a total of 12 devices were fabricated. In these devices, indium tin oxide (ITO) is used as the anode, 4,4',4''-tris[N-(1-naphthyl)-N-phenylamino]triphenylamine (2-TNATA) or MoO3 are used as the hole-injection layer, 4,4-bis[N-(1-naphthyl)-N-phenyl-1-amino]biphenyl (NPB) is used as the hole transporting layer (HTL), tris(8-hydroxy-quinolino)aluminum (Alq3) or 1,3,5-tris(1-phenyl-1H-benzimidazol-2-yl)benzene (TPBI) are used as the electron transporting

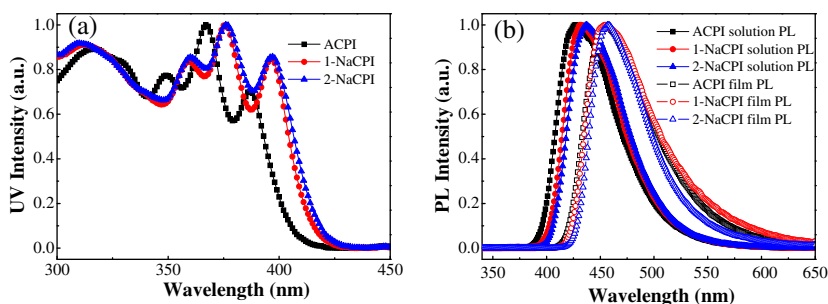


Fig. 4. (a) Normalized absorption spectra of compound ACPI, 1-NaCPI and 2-NaCPI in dichloromethane; (b) normalized photoluminescence spectra in dichloromethane and film state.

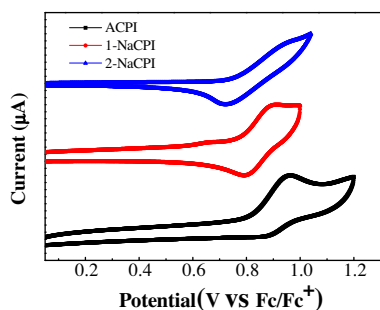


Fig. 5. The CV measurement of ACPI, 1-NaCPI and 2-NaCPI.

layer (ETL), and $(\text{CH}_3)_3\text{CCOOCs}$ is used as the electron injecting layer [17]. The relative HOMO/LUMO energy levels of the materials are illustrated in Scheme 2, and detailed structures and key performance of the 12 devices are summarized in Table 2.

Non-doped devices 1, 2 and 3 were fabricated with typical configuration as follows: ITO/2-TNATA(60 nm)/NPB (10 nm)/emitting layer (40 nm)/Alq3 (15 nm)/ $(\text{CH}_3)_3\text{CCOOCs}$ (2 nm)/Al (100 nm). The current density–voltage–luminance (I–V–L) and current density–current efficiency characteristics are shown in Fig. 6. Simple devices 1, 2, 3 utilizing compounds ACPI, 1-NaCPI and 2-NaCPI as host exhibit a maximum brightness of 18,460, 16,000, and 12,250 cd m^{-2} , luminous efficiency of 4.62, 4.36, 4.65 cd A^{-1} , low threshold voltage of 2.83, 2.73, 2.71 V, respectively (see Table 2). The low turn on voltage can be attributed to the fact that reasonable HOMO level of the compounds reduce the hole injection barrier at the interface between the hole-transporting layer and the emissive layer. The EL spectra of 1, 2 and 3 show blue light emission with peaks at 472, 468 and 460 nm, respectively (Fig. 7(a)). Narrow EL peaks in the ACPI, 1-NaCPI and 2-NaCPI devices with FWHMs of 77, 72 and 61 nm, respectively, are observed. At a current density of 20 mA cm^{-2} , the CIE coordinates of devices 1, 2 and 3 are (0.1560, 0.2168), (0.1655, 0.1996) and (0.1505, 0.1605), respectively (see Table 2). The EL spectra of the devices fabricated using ACPI and 1-NaCPI as the emitting layers have a little red shift compared to 2-NaCPI. It may be ascribed to a slight contribution from Alq3 emission [18].

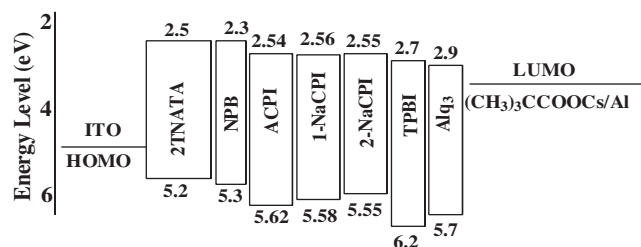
In order to confirm the above hypothesis, devices 4, 5 and 6 for ACPI, 1-NaCPI and 2-NaCPI with the same configuration as follows: ITO/2-TNATA (60 nm)/NPB (10 nm)/emitting layer (40 nm)/TPBI (15 nm)/ $(\text{CH}_3)_3\text{CCOOCs}$

(2 nm)/Al (100 nm), were fabricated for further evaluation of EL performances. Since TPBI has lower HOMO of 6.2 V, using TPBI as electron transport material to instead Alq3, can prevent the injection of hole into Alq3 and avoid the emission of Alq3.

As predicted, the CIE of devices 4, 5 shifted to blue obviously (see Fig 7(b)) when using TPBI to instead of Alq3, from (0.1560, 0.2168) to (0.1562, 0.1551), from (0.1655, 0.1996) to (0.1503, 0.1669), respectively. However, for the compound 2-NaCPI, the CIE exhibits negligible change, from (0.1505, 0.1605) to (0.1508, 0.1573). These phenomena can be explained from the energy diagrams, the HOMO level gap in Alq3/EML interface (0.08, and 0.12 eV for ACPI, 1-NaCPI, respectively) is too small to block the diffusion of exciton, especially for ACPI. Meanwhile, narrower EL peaks in the devices 4, 5 and 6 with FWHMs of 65, 71 and 59 nm respectively, (see Fig. 7), which is almost correlated with the PL in solid state. With respect to devices 4, 5 and 6, TPBI acts both as an electron-transporter and as a hole-blocking layer, and the exciton can be confined to the emissive layer efficiently. Noteworthy, whether the electron transporting layer is Alq3 or TPBI, 2-NaCPI exhibits high efficiency, and pure blue light emission in the device due to its suitable HOMO level. Fig. 8 reveals the current density–current efficiency characteristics of devices 4, 5 and 6. Devices 4, 5 and 6 exhibit a maximum brightness of 11,470, 14,680, and 11,840 cd m^{-2} , and luminous efficiency of 4.36, 4.22, 4.68 cd A^{-1} , respectively (see Table 2). For ACPI and 2-NaCPI, the maximum power efficiency was enhanced to 3.03 and 3.6 lm W^{-1} . We attribute this enhancement to the better electron transporting ability of TPBI.

To explore the possible electron transporting properties of these materials, a bilayer device 7, 8, 9 with a structure of ITO/2-TNATA (60 nm)/NPB (10 nm)/ACPI, 1-NaCPI or 2-NaCPI (60 nm)/ $(\text{CH}_3)_3\text{CCOOCs}$ (2 nm)/Al (100 nm) were also fabricated. Here, ACPI, 1-NaCPI or 2-NaCPI was used as both the ETL and the emitter. Devices 7, 8 and 9 exhibit a maximum brightness of 10,570, 11,650, and 15,030 cd mA m^{-2} , and luminous efficiency of 3.32, 2.52, 3.64 cd A^{-1} , the CIE coordinates of (0.1573, 0.1529), (0.1531, 0.1711), (0.1603, 0.1879), respectively (see Table 2). Compared with Alq3 based devices 1, 2 and 3, the contiguous numerical value of working voltage suggests that these materials are an electron-transporting type blue host material.

For organic semiconductors, conductivities of emissive materials with electron-transport properties are generally



Scheme 2. Energy-level diagram of the materials used in the devices.

Table 2
EL performance of devices 1–12.

Device	V_{on} (V) ^a	L_{max} (Voltage) (cd m ⁻²) ^b	η_p (lm W ⁻¹) ^{c, d}	η_c (cd A ⁻¹) ^{e, f}	η_{ext} (%) ^{g, h}	L (Voltage) (cd m ⁻²) ⁱ	λ_{em} (FWHM) (nm) ^j	CIE (x,y) ^k
1	2.83	18,460 (10.80)	2.29 (2.96)	4.30 (4.62)	2.72 (3.02)	860 (5.91)	472 (77)	(0.1560, 0.2168)
2	2.73	16,000 (10.50)	2.46 (3.22)	4.32 (4.36)	2.82 (2.88)	864 (5.52)	468 (72)	(0.1655, 0.1996)
3	2.71	12,250 (10.30)	2.48 (3.18)	4.63 (4.65)	3.59 (3.61)	926 (5.87)	460 (61)	(0.1505, 0.1605)
4	2.76	11,470 (8.25)	2.55 (3.03)	4.17 (4.36)	3.27 (3.52)	834 (5.13)	456 (65)	(0.1562, 0.1551)
5	3.07	14,680 (10.50)	2.12 (2.46)	4.13 (4.22)	3.13 (3.23)	826 (6.11)	468 (71)	(0.1503, 0.1669)
6	2.66	11,840 (9.25)	2.95 (3.60)	4.67 (4.68)	3.65 (3.68)	934 (5.01)	460 (59)	(0.1508, 0.1573)
7	3.03	10,570 (8.50)	1.89 (2.13)	3.10 (3.32)	2.46 (2.73)	620 (5.15)	456 (66)	(0.1573, 0.1529)
8	2.86	11,650 (10.50)	1.35 (1.42)	2.45 (2.52)	1.83 (1.89)	490 (5.69)	468 (65)	(0.1531, 0.1711)
9	2.76	15,030 (9.75)	2.06 (2.59)	3.61 (3.64)	2.47 (2.52)	722 (5.52)	468 (63)	(0.1603, 0.1897)
10	3.05	7357 (7.50)	0.94 (1.36)	1.50 (1.59)	1.04 (1.16)	300 (4.99)	456 (70)	(0.1699, 0.1774)
11	2.96	3153 (11.00)	0.48 (0.78)	0.86 (0.93)	0.64 (0.69)	172 (5.50)	468 (65)	(0.1578, 0.1658)
12	2.90	7109 (11.00)	0.85 (1.40)	1.64 (1.72)	0.99 (1.03)	328 (6.08)	468 (67)	(0.1916, 0.2267)

^a V_{on} : turn-on voltage.

^b L_{max} : maximum luminance. Voltage: voltage at the maximum luminance.

^c η_p : power efficiency measured at 20 mA cm⁻².

^d Maximum power efficiency.

^e η_c : current efficiency measured at 20 mA cm⁻².

^f Maximum current efficiency.

^g η_{ext} : external quantum efficiency measured at 20 mA cm⁻².

^h Maximum external quantum efficiency.

ⁱ L : luminance measured at 20 mA cm⁻². Voltage: voltage at the luminance.

^j λ_{em} : FWHM: full width at half maximum at 20 mA cm⁻².

^k λ_{em} : CIE at 20 mA cm⁻².

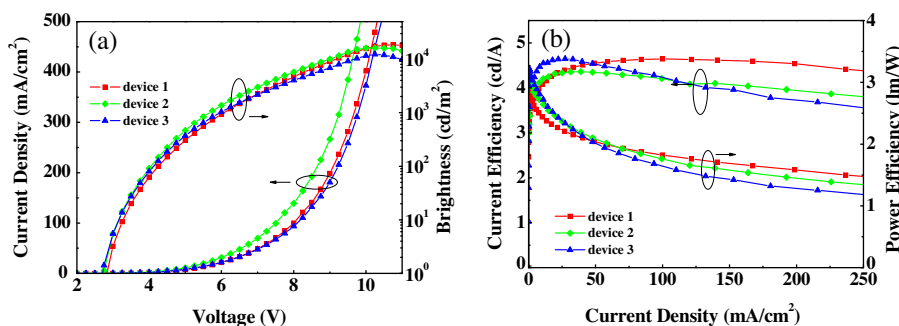


Fig. 6. (a) Voltage–current density–luminance (V – J – L) characteristics and (b) efficiencies curves for blue devices 1, 2 and 3. (For interpretation of the references to colour in this figure legend, the reader is referred to the web version of this article.)

lagging behind those materials with hole-transport properties. So it is possible to construct a single layer device using the electron-type material. In order to verify the hypothesis, a single layer device 10, 11, 12 with a structure of ITO/MoO₃ (10 nm)/ACPI, 1-NaCPI or 2-NaCPI (100 nm)/(CH₃)₃CCOOCs (2 nm)/Al (100 nm) were also fabricated. Devices 10, 11 and 12 exhibit a maximum brightness of 7357, 3153, and 7109 cd m⁻², and luminous efficiency of

1.59, 0.93, 1.72 cd A⁻¹, the CIE coordinates of (0.1699, 0.1774), (0.1578, 0.1658), (0.1916, 0.2267), respectively (see Table 2). Compared to the multilayer devices, part of CIE coordinates of single device has changed obviously, it may be caused by the intermolecular interactions and the thickness of emitting layer, and the same phenomena were also observed in the reported single layer device [5g]. Clearly, the maximum efficiencies of these single devices

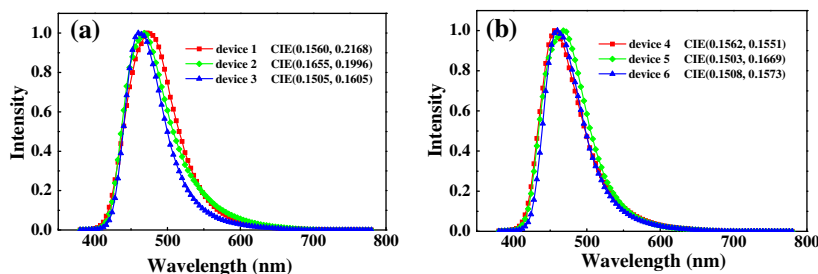


Fig. 7. (a) EL spectrum of devices 1, 2 and 3 and (b) EL spectrum of devices 4, 5 and 6.

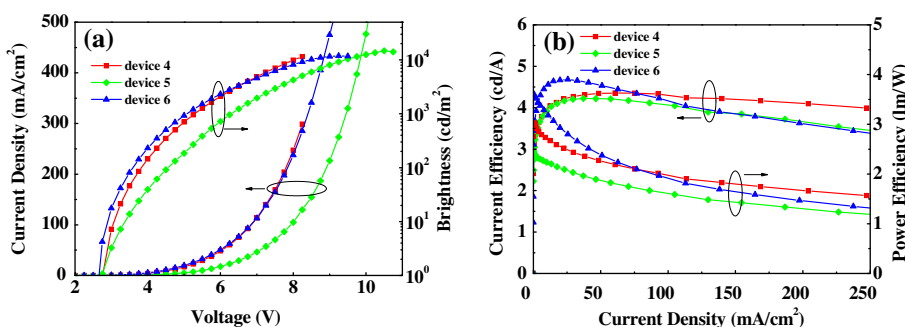


Fig. 8. (a) Voltage–current density–luminance (V – J – L) characteristics and (b) efficiencies curves for blue devices 4, 5 and 6. (For interpretation of the references to colour in this figure legend, the reader is referred to the web version of this article.)

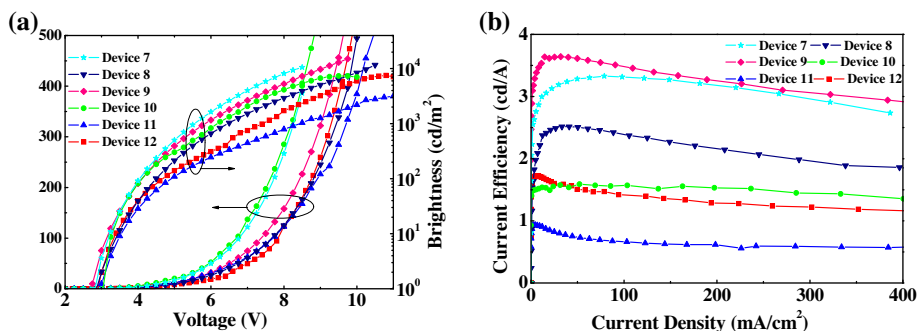


Fig. 9. (a) Voltage–current density–luminance (V – J – L) characteristics and (b) efficiencies curves for devices 7–12.

are below those of the bilayer and trilayer devices (devices 1–9). Devices 10 and 12 showing better performance than device 11 could be attributed more large steric hindrance of 1-NaCPI which will reduce its electron-transporting ability [14]. On the other hand, it is worth noting that all the single layer devices show little efficiency roll-off as current density increases (Fig. 9).

To further access the performance of ACPI as a blue emitter, performance of device 4 was compared with those of similarly structured blue emitting devices reported recently (Table 3) [6,7,19–24]. Device 4 has negligible efficiency roll off at high current densities. Such as, compared to the maximum current efficiency, the efficiency roll off of device 4 is only 8.2% when the current density increased to 200 cd A^{-1} . By the way, it can be seen from the Table 3 that

the performance of the ACPI based devices are comparable in terms of turn-on voltage, luminance and efficiency and efficiency roll off to anthracene-based non-doped devices with CIE $x + y \sim 0.30$ [6,7,19–24].

4. Conclusions

In summary, a series of new robust blue fluorescence materials were developed based on anthracene and phenanthro[9,10-d]imidazole functional cores. These compounds with fitly energy levels and increasing electron transport ability, exhibit strong blue emission in both solid state and EL device. Non-doped device 4 using ACPI as the emitting layer, its maximum electroluminescence effi-

Table 3Key characteristics of devices **4** and other recently reported anthracene-based non-doped blue emitting devices with CIE $x + y \sim 0.3$.

Emitter	V_{on}^a (V)	η_c^{maxc} ($cd A^{-1}$)	η_c^{200} ($cd A^{-1}$)	$\eta_c^{roll off}$ (%)	η_p^{max} ($lm W^{-1}$)	CIE (x, y)	Moiety	L_{max}^c ($cd m^{-2}$)	Refs.
ACPI	2.76	4.36	4.0	8.2	3.03	(0.156, 0.155) ^d	Phenanthroimidazole	11,470	Device 4
TPVAn	4.9	5.3	3.2	39.6	na	(0.14, 0.12)	Tetraphenylethylene	No	[4a]
P-DAC	3.8	3.14	3.16	+2	0.92 ^e	(0.16, 0.14)	Carbazole	na	[6]
NAF1	4.1	4.04	2.6	35.6	2.20	(0.15, 0.13)	Fluorene	6528	[7]
TPA-AN	na	4.54	3.7	18.5	4.02 ^f	(0.15, 0.19)	Arylamine	24,910	[19]
tCz ⁹ Ph ₂ Ant	5.5	2.10	1.2	42.8	na	(0.17, 0.16)	Carbazole	1576	[20]
4	4.6	1.65	1.4	15.2	na	(0.15, 0.16)	Fluorene, arylamine	4586	[21]
NPAT	5.9	2.98	na	na	1.52	(0.15, 0.14)	Truxene	1318	[22]
2	4.6 ^b	1.65	na	na	na	(0.15, 0.16)	Fluorene, arylamine	4586	[23]
DPAPFB	6.5	5.1	3.9	23.5	1.10	(0.18, 0.21)	Fluorene	12,508	[24]

Part of data was obtained from the figure of the reference.

^a V_{on} : onset voltage obtained at $1 cd m^{-2}$.^b Obtained at $10 cd m^{-2}$.^c η_c^{max} , η_c^{200} , η_p^{max} and L_{max} are maximum current efficiency, current efficiency at $200 mA cm^{-2}$, power efficiency and luminance respectively.^d Obtained at $20 mA cm^{-2}$.^e Obtained at $100 mA cm^{-2}$.^f PEDOT:PSS inserted.

ciency reaches $4.36 cd A^{-1}$ with Commission Internationale del'Eclairage (CIE) coordinates of (0.156, 0.155). In the single layer device **10**, its maximum efficiency reaches $1.59 cd A^{-1}$ with Commission Internationale del'Eclairage (CIE) coordinates of (0.169, 0.177). Interestingly, both device **4** and **10** has negligible efficiency roll off at high current densities, which is among the best reported results for anthracene-based nondoped simple devices.

Acknowledgments

This work was supported by Wuhan Science and Technology Bureau (01010621227), the Doctoral Fund of the Ministry of Education of China (20100142120049) and NSFC/China (21161160442).

Appendix A. Supplementary data

Supplementary data associated with this article can be found, in the online version, at <http://dx.doi.org/10.1016/j.orgel.2012.08.032>.

References

- [1] C.W. Tang, S.W. Vanslyke, *Appl. Phys. Lett.* 51 (1987) 913.
- [2] (a) B.W. D'Andrade, S.R. Forrest, *Adv. Mater.* 16 (2004) 1585; (b) M.C. Gather, A. Köhnen, K. Meerholz, *Adv. Mater.* 23 (2011) 233.
- [3] Y.H. Chen, H.H. Chou, T.H. Su, P.Y. Chou, F.I. Wu, C.H. Cheng, *Chem. Commun.* 47 (2011) 8865.
- [4] (a) P.I. Shih, C.Y. Chuang, C.H. Chien, D.E. Wei-Guang, C.F. Shu, *Adv. Funct. Mater.* 17 (2007) 3141; (b) R.C. Chiechi, R.J. Tseng, F. Marchioni, Y. Yang, F. Wudl, *Adv. Mater.* 18 (2006) 325; (c) S. Tang, M.R. Liu, P. Lu, H. Xia, M. Li, Z.Q. Xie, F.Z. Shen, C. Gu, H. Wang, B. Yang, Y.G. Ma, *Adv. Funct. Mater.* 17 (2007) 2869.
- [5] (a) C.H. Chien, C.K. Chen, F.M. Hsu, C.F. Shu, P.T. Chou, C.H. Lai, *Adv. Funct. Mater.* 19 (2009) 560; (b) C.H. Wu, C.H. Chien, F.M. Hsu, P.I. Shih, C.F. Shu, *J. Mater. Chem.* 19 (2009) 1464; (c) C.J. Zheng, W.M. Zhao, Z.Q. Wang, D. Huang, J. Ye, X.M. Ou, X.H. Zhang, C.S. Lee, S.T. Lee, *J. Mater. Chem.* 20 (2010) 1560; (d) K.R. Wee, W.S. Han, J.E. Kim, A.L. Kim, S. Kwon, S.O. Kang, *J. Mater. Chem.* 21 (2011) 1115; (e) K.H. Lee, J.K. Park, J.H. Seo, S.W. Park, Y.S. Kim, Y.K. Kim, S.S. Yoon, *J. Mater. Chem.* 21 (2011) 13640; (f) S.H. Lin, F.I. Wu, H.Y. Tsai, P.Y. Chou, H.H. Chou, C.H. Cheng, R.S. Liu, *J. Mater. Chem.* 21 (2011) 8122; (g) J.H. Huang, J.H. Su, X. Li, M.K. Lam, K.M. Fung, H.H. Fan, K.W. Cheah, C.H. Chen, H. Tian, *J. Mater. Chem.* 21 (2011) 2957.
- [6] S.H. Kim, I. Cho, M.K. Sim, S. Park, S.Y. Park, *J. Mater. Chem.* 21 (2011) 9139.
- [7] T. Zhang, D. Liu, Q. Wang, R.J. Wang, H.C. Renb, J.Y. Li, *J. Mater. Chem.* 21 (2011) 12969.
- [8] C.J. Kuo, T.Y. Li, C.C. Lien, C.H. Liu, F.I. Wub, M.J. Huang, *J. Mater. Chem.* 19 (2009) 1865.
- [9] Z.M. Wang, P. Lu, S.M. Chen, Z. Gao, F.Z. Shen, W.S. Zhang, Y.X. Xu, H.S. Kwokb, Y.G. Ma, *J. Mater. Chem.* 21 (2011) 5451.
- [10] H. Huang, Q. Fu, S.Q. Zhuang, Y.K. Liu, L. Wang, J.S. Chen, D.G. Ma, C.L. Yang, *J. Phys. Chem. C* 115 (2011) 4872.
- [11] (a) L. Wang, Z.Y. Wu, W.Y. Wong, K.W. Cheah, H. Huang, C.H. Chen, *Org. Electron.* 12 (2011) 595; (b) H. Huang, Q. Fu, S.Q. Zhuang, G.Y. Mu, L. Wang, J.S. Chen, D.G. Ma, C.L. Yang, *Org. Electron.* 12 (2011) 1716.
- [12] (a) Y. Yuan, D. Li, X.Q. Zhang, X.J. Zhao, Y. Liu, J.Y. Zhang, Y. Wang, *New J. Chem.* 35 (2011) 1534; (b) Y. Zhang, S.L. Lai, Q.X. Tong, M.Y. Chan, T.W. Ng, Z.C. Wen, G.Q. Zhang, S.T. Lee, H.L. Kwong, C.S. Lee, *J. Mater. Chem.* 21 (2011) 8206; (c) Y. Zhang, S.L. Lai, Q.X. Tong, M.F. Lo, T.W. Ng, M.Y. Chan, T.W. Ng, Z.C. Wen, J. He, K.S. Jeff, X.L. Tang, W.M. Liu, C.C. Ko, P.F. Wang, C.S. Lee, *Chem. Mater.* 24 (2012) 61.
- [13] S. Hamal, F. Hirayama, *J. Phys. Chem.* 87 (1983) 83.
- [14] L. Wang, W.Y. Wong, M.F. Lin, W.K. Wong, K.W. Cheah, H.L. Tam, C.H. Chen, *J. Mater. Chem.* 18 (2008) 4529.
- [15] J.Y. Li, D. Liu, C. Ma, O. Lengyel, C.S. Lee, C.H. Tung, S.T. Lee, *Adv. Mater.* 16 (2004) 1538.
- [16] C.H. Chen, *Organic Electroluminescent Materials and Devices*, Tsinghua University, China, 2005.
- [17] R.G. Shangguan, G.Y. Mu, X.F. Qiao, L. Wang, K.W. Cheah, X.J. Zhu, C.H. Chen, *Org. Electron.* 12 (2011) 1957.
- [18] L. Duan, D.Q. Zhang, K.W. Wu, X.Q. Huang, L.D. Wang, Y. Qiu, *Adv. Funct. Mater.* 21 (2011) 3540.
- [19] S. Tang, W.J. Li, F.Z. Shen, D.D. Liu, B. Yang, Y.G. Ma, *J. Mater. Chem.* 22 (2012) 4401.
- [20] Y.H. Chen, S.L. Lin, Y.C. Chang, Y.C. Chen, J.T. Lin, R.H. Lee, W.J. Kuo, R.J. Jeng, *Org. Electron.* 13 (2012) 43.
- [21] A. Thangthong, D. Meunmart, N. Prachumrak, S. Jungstittiwong, T. Keawin, T. Sudyoadsuk, V. Promarak, *Tetrahedron* 68 (2012) 1853.
- [22] J.H. Huang, B. Xu, J.H. Su, C.H. Chen, H. Tian, *Tetrahedron* 66 (2010) 7577.
- [23] A. Thangthong, D. Meunmart, N. Prachumrak, S. Jungstittiwong, T. Keawin, T. Sudyoadsuk, V. Promarak, *Chem. Commun.* 47 (2011) 7122.
- [24] S.H. Ye, J.M. Chen, C.A. Di, Y.Q. Liu, K. Lu, W.P. Wu, C.Y. Du, Y. Liu, Z.G. Shuai, G. Yu, *J. Mater. Chem.* 20 (2010) 3186.